



Polarimetric radar cross section under SAR geometry

N. Phruksahiran and M. Chandra

Professorship of Microwave Engineering and Electromagnetic Theory, Chemnitz University of Technology, Germany

Correspondence to: N. Phruksahiran (narathep.phruksahiran@s2009.tu-chemnitz.de)

Abstract. In this paper, the radar cross section of canonical scatter, with perfectly conducting surface, under the synthetic aperture radar geometry and polarized electromagnetic wave, has been considered and a new approach of polarized scattered electric field approximation for its evaluation has been developed.

1 Introduction

The synthetic aperture radar (SAR) system works by transmitting electromagnetic waves to the area of interest to survey or surveillance in case of disaster monitoring. The electromagnetic wave signals can be modified or modulated to increase the resolution in the range direction. The key feature of the electromagnetic wave which used in polarimetric SAR system is the property of different reflection or scattering mechanism depending on different types of the subject or target by using the polarization of transmitted and received wave.

The level or the strength of the reflected electromagnetic wave signal are different and are based on the roughness of the surface, the distance and the structure of the target on the ground. There are many researchers, who try to simulate and to do experiments about the reflection of electromagnetic waves from various objects.

In this paper, we present a new approach to calculate the polarimetric radar cross section of canonical targets which represent the structure of the ground surface, e.g., the flat plate, the dihedral reflector and the trihedral reflector represent the flat surface, the fence along the border wall or forest and the urban structure, respectively. The radar cross section was determined under the SAR geometry and polarization of incident and scattered electric fields by using physical optic approximation and far field radiation.

This paper is organized as follows. In Sect. 2, we review some basic and the mathematical definitions of the scattering process, the radar cross section and the simulation of scat-

tered fields using physical optic approximation. The new approaches of polarimetric radar cross section are presented in Sect. 3. The experimental model, i.e., the ground based SAR geometry which was used in this paper and the target model, are presented in Sect. 4. In Sect. 5, we present the simulation results of the flat plate, the dihedral reflector and the trihedral reflector. The conclusion is addressed in Sect. 6.

2 Basics

The scattering mechanism of the object in far field can be modeled as a linear transformation between incident electric fields E^i and scattered electric fields E^s , described by a scattering matrix S_{pq} as shown by Lee and Pottier (2009):

$$E^s = \frac{e^{-jkR}}{R} [S_{pq}] E^i \quad (1)$$

or

$$E^s = \begin{bmatrix} E_h^s \\ E_v^s \end{bmatrix} = \frac{e^{-jkR}}{R} \begin{bmatrix} S_{hh} & S_{hv} \\ S_{vh} & S_{vv} \end{bmatrix} \begin{bmatrix} E_h^i \\ E_v^i \end{bmatrix}. \quad (2)$$

Where the distance between the antenna and the scattering object is R , k is the wavenumber. The term e^{-jkR}/R describes the wave propagation effects in amplitude and in phase. The parameters S_{pq} are the complex scattering amplitude element of the scattering matrix $[S_{pq}]$, in which the index q and p stand for the incident and scattered polarization, respectively. The index h and v denote the horizontal and vertical polarization basis of the wave.

2.1 Radar cross section

The reflected signal from an object contains valuable information about the target object itself. The radar cross section and the reflectivity are important for the SAR signal processing and for further evaluation in the image data. The radar cross section is an important target property described as a

effective surface which describes the electromagnetic reflectivity of the target in the direction back to the radar. It depends on target structure, the frequency of signal and the polarization of incident and scattered electrical fields. The radar cross section is generally defined by using power comparison between the incident wave and the reflected wave and can be calculated as follows:

$$\sigma_{pq} = \lim_{R \rightarrow \infty} 4\pi R^2 \frac{|\mathbf{E}_p^s(\theta_s, \phi_s)|^2}{|\mathbf{E}_q^i(\theta_i, \phi_i)|^2} \quad (3)$$

The angle designation $\theta_i, \theta_s, \phi_i$ and ϕ_s are presented in Fig. 1 by using the Cartesian coordinate system \hat{x}, \hat{y} and \hat{z} axis. It shows the direction of incident and scattered electric fields which was used in this paper. The angle θ_i is between the \hat{z} axis and the incident direction of the wave. The angle θ_s is between the \hat{z} axis and the scattered direction of the wave. The angle ϕ_i and ϕ_s can be determined by using the projection on the xy-plane with respect to the \hat{x} axis.

The components of scattering matrix $[\mathbf{S}_{pq}]$ are related to polarimetric radar cross section σ_{pq} and can be determined from the Eqs. (1) and (3) as follows:

$$\sigma_{pq} = 4\pi |\mathbf{S}_{pq}|^2 \quad (4)$$

2.2 Simulation of scattered fields using physical optic

In practice, the reflection on the perfectly conducting metal surface is considered. An important role is to determine the interaction between the incident waves and the scattering mechanism on the surface. In the physical optic approximation, it can be assumed that the tangential component of the reflected magnetic field strength is equal to the tangential component of the incident magnetic field strength. So that the relationship between the current distribution on the scattering surface \mathbf{J}_s , the incident magnetic field \mathbf{H}^i and the unit vector normal to the scatter surface \hat{n} as shown by Balanis (1989):

$$\mathbf{J}_s = 2\hat{n} \times \mathbf{H}^i \quad (5)$$

The evaluation of the scattered electric field can be done by using the magnetic flux density \mathbf{B} and the vector potential \mathbf{A} with $\mathbf{B} = \nabla \times \mathbf{A}$. By solving the Maxwell's equation and definition of vector notation with $\mathbf{r} = (x\hat{x} + y\hat{y} + z\hat{z})$ for observation point, $\mathbf{r}' = (x'\hat{x} + y'\hat{y} + z'\hat{z})$ for source point and ψ as the angel between vector \mathbf{r} and \mathbf{r}' , we get using $R = r - r' \cos \psi$:

$$\begin{aligned} \mathbf{A}(x, y, z) &= \frac{\mu}{4\pi} \int_S \mathbf{J}_s(x', y', z') \frac{e^{-jkR}}{R} ds' \\ &\approx \frac{\mu e^{-jkr}}{4\pi r} \mathbf{N} \end{aligned} \quad (6)$$

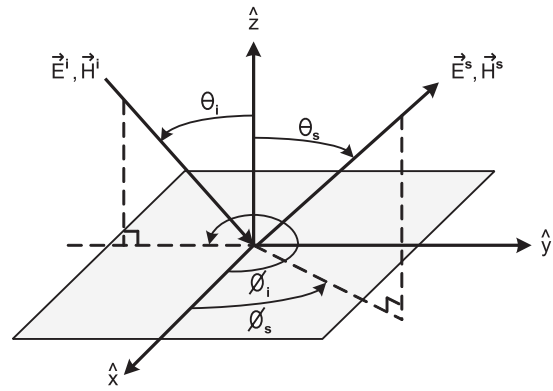


Fig. 1. Angle representation for the incident and scattered electrical fields.

with

$$\mathbf{N} = \int_S \mathbf{J}_s(x', y', z') e^{jkr' \cos \psi} ds' \quad (7)$$

The scattered electric field \mathbf{E}^s in the far field region can be calculated from the vector-potential \mathbf{A} and the angular frequency ω as:

$$\mathbf{E}^s = -j\omega \mathbf{A} \quad (8)$$

To a good approximation in the spherical coordinate system $(\hat{r}, \hat{\theta}, \hat{\phi})$, the components of the scattered electric field can be assumed as follows:

$$E_r^s \approx 0 \quad (9)$$

$$E_\theta^s \approx -\frac{jke^{-jkr}}{4\pi r} \eta N_\theta \quad (10)$$

$$E_\phi^s \approx -\frac{jke^{-jkr}}{4\pi r} \eta N_\phi \quad (11)$$

Where η is the impedance of free space. By using the coordinate transformation, the parameters N_θ and N_ϕ in the spherical coordinate system can be described from the parameters J_x, J_y and J_z in the Cartesian coordinate system as:

$$\begin{aligned} N_\theta &= \int_S \int_S (J_x \cos \theta_s \cos \phi_s + J_y \cos \theta_s \sin \phi_s - J_z \sin \theta_s) \\ &\quad \cdot e^{jkr' \cos \psi} ds' \end{aligned} \quad (12)$$

$$N_\phi = \int_S \int_S (-J_x \sin \phi_s + J_y \cos \phi_s) e^{jkr' \cos \psi} ds' \quad (13)$$

3 Polarimetric radar cross section approach

In this paper, the electromagnetic interaction was considered in horizontal and vertical polarization. The new approach

taken converts the electric field components, which can be calculated in spherical coordinate system, into the electric field components in Cartesian coordinate system as follows:

$$E_x^s = E_r^s \sin \theta_s \cos \phi_s + E_\theta^s \cos \theta_s \cos \phi_s - E_\phi^s \sin \phi_s \quad (14)$$

$$E_y^s = E_r^s \sin \theta_s \sin \phi_s + E_\theta^s \cos \theta_s \sin \phi_s + E_\phi^s \cos \phi_s \quad (15)$$

$$E_z^s = E_r^s \cos \theta_s - E_\theta^s \sin \theta_s \quad (16)$$

The y component and the z component of the scattered electric fields are used for the horizontal and the vertical received mode, respectively, so that we can define the polarized radar cross section as follows:

$$\sigma_{hh}(u, r) = 4\pi r^2 \frac{|E_h^s(\theta_s, \phi_s)|^2}{|E_h^i(\theta_i, \phi_i)|^2} = 4\pi r^2 \frac{|E_y^s(\theta_s, \phi_s)|^2}{|E_h^i(\theta_i, \phi_i)|^2} \quad (17)$$

$$\sigma_{vh}(u, r) = 4\pi r^2 \frac{|E_v^s(\theta_s, \phi_s)|^2}{|E_h^i(\theta_i, \phi_i)|^2} = 4\pi r^2 \frac{|E_z^s(\theta_s, \phi_s)|^2}{|E_h^i(\theta_i, \phi_i)|^2} \quad (18)$$

$$\sigma_{hv}(u, r) = 4\pi r^2 \frac{|E_h^s(\theta_s, \phi_s)|^2}{|E_v^i(\theta_i, \phi_i)|^2} = 4\pi r^2 \frac{|E_y^s(\theta_s, \phi_s)|^2}{|E_v^i(\theta_i, \phi_i)|^2} \quad (19)$$

$$\sigma_{vv}(u, r) = 4\pi r^2 \frac{|E_v^s(\theta_s, \phi_s)|^2}{|E_v^i(\theta_i, \phi_i)|^2} = 4\pi r^2 \frac{|E_z^s(\theta_s, \phi_s)|^2}{|E_v^i(\theta_i, \phi_i)|^2} \quad (20)$$

The parameter u represents the position of the radar antenna along the flight line as shown in Fig. 2.

4 Experiment model

In this section, the geometry of the numerical calculations of the cross sections of the canonical target objects under the ground-based SAR and the target modeling are defined and presented.

4.1 Ground based SAR geometry

Figure 2 shows the geometry of ground based SAR system and the radar parameter. Where $L = 10$ m is the length of the rail of the radar, u defines the radar position, $h = 30$ m is the height of the building, R_0 is the range of closest approach, $\beta_r = 45^\circ$ is the off nadir angel. At sensor position A, the target is just entering the radar beam and leaves the radar beam at position C. At position B, the point target lines in the center of the beam.

The special property of SAR system is, for different positions of radar during the observation interval, the angle theta and phi, the component of magnetic field and the direction of incident and scattered field at the target are changed continuously which has to be taken into account by numerical calculations.

4.2 Target modell and numerical calculation

Figure 3a–c present the canonical targets considered in this paper. The calculation for the flat plate consists of only one

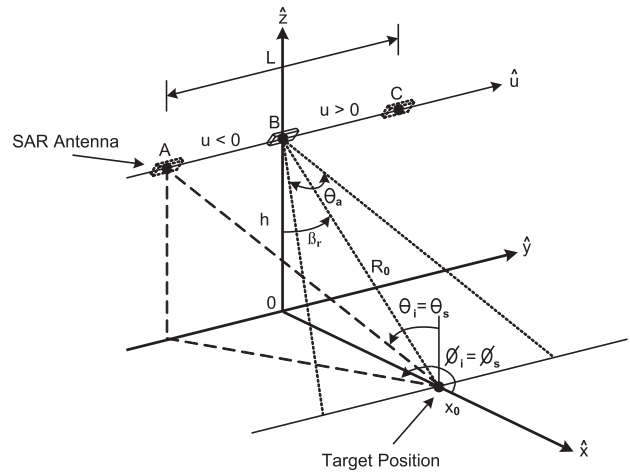


Fig. 2. Experiment Modell with Ground Based SAR Geometry.

reflection on the surface. In case of dihedral reflector and trihedral reflector, we include the doubly reflected fields and triply reflected fields between each plate of the reflector into account. In this paper we consider only the interaction between the plates without the diffracted field from the exterior edges. The main goal is the calculation of the current density of the interaction between the incident magnetic field and the surface. Then the scattered electric field can be calculated with the help of the vector potential that is related to the current density and magnetic field.

4.2.1 Flat plate

The calculation for the flat plate consists of only one scattering mechanism on the surface, as shown in Fig. 4. The method of physical optics is used to determine the surface current distribution arising from the incident magnetic field.

4.2.2 Dihedral

A dihedral corner reflector can be considered as a composition of two flat plates that are perpendicular to each other. From the geometry of the dihedral corner reflector, the numerical calculations of scattered electric field are divided into three groups as follows: Fig. 5a shows the case R_1 of singly reflected field from plate Nr. 1. The case R_{21} is presented in Fig. 5b which can be calculated with PO-PO methodology. In this case the incident magnetic field on plate Nr. 1 induces the surface current density J_{s1} that generates the magnetic field H_{s2} on plate Nr. 2. The surface current density J_{s2} on plate Nr. 2 can be calculated with PO. Figure 5c shows the case R_{121} of triply reflected field in which the first reflection from plate Nr. 1 to plate Nr. 2 can be calculated by using geometrical optics (GO) method. In this case the incident magnetic field on plate Nr. 2 induces the surface current density J_{s2} that generates the magnetic field H_{s1} on plate Nr. 1. The

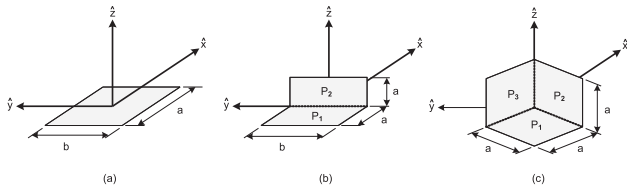


Fig. 3. Target Modell (a) flat plate; (b) dihedral reflector; (c) trihedral reflector.

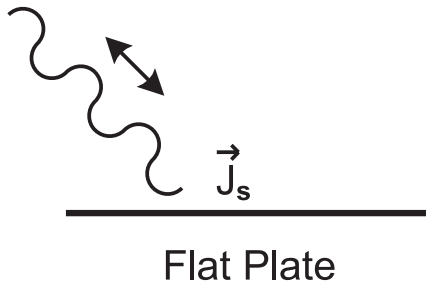


Fig. 4. Numerical calculation for flat plate.

surface current density J_{s1} on plate Nr. 1 can be calculated with PO. The total cases of reflected fields of dihedral corner reflector are $R_1, R_2, R_{21}, R_{12}, R_{121}$ and R_{212} .

4.2.3 Trihedral

From the geometry of the trihedral corner reflector as shown in Fig. 3c, the numerical calculations of scattered electric field can be divided into three groups like the dihedral corner reflector as follows: Fig. 6a shows the case R_1 of singly reflected field from plate Nr. 1 that can be determined with PO. Figure 6b presents the case R_{21} that can be calculated with PO-PO methodology. In this case the incident magnetic field on plate Nr. 1 induces the surface current density J_{s1} that generates the magnetic field H_{s2} on plate Nr. 2. The surface current density J_{s2} on plate Nr. 2 can be calculated with PO to get the scattered electric field in far field. Figure 6c shows the case R_{121} of triply reflected field in which the first reflection from plate Nr. 1 to plate Nr. 2 can be calculated by using geometrical optics (GO) method. In this case the incident magnetic field on plate Nr. 2 induces the surface current density J_{s2} that generates the magnetic field H_{s1} on plate Nr. 1. The surface current density J_{s1} on plate Nr. 1 can be determined with PO. The total cases of reflected fields of trihedral corner reflector are $R_1, R_2, R_3, R_{21}, R_{31}, R_{12}, R_{32}, R_{13}, R_{23}, R_{121}, R_{321}, R_{131}, R_{231}, R_{212}, R_{312}, R_{132}, R_{232}, R_{213}, R_{313}, R_{123}$ and R_{323} .

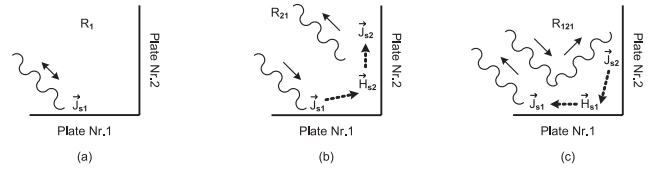


Fig. 5. Numerical calculation for dihedral corner reflector with (a) Singly reflected fields; (b) Doubly reflected fields; (c) Triply reflected fields.

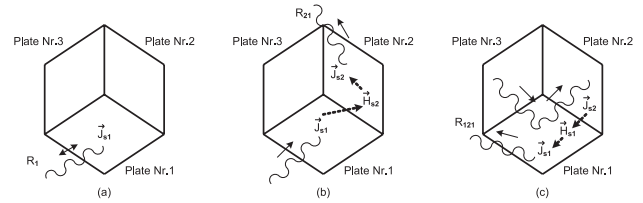


Fig. 6. Numerical calculation for trihedral corner reflector with (a) Singly reflected fields; (b) Doubly reflected fields; (c) Triply reflected fields.

5 Results

This section presents the simulation results of polarimetric radar cross section with $a = 1$ m and $b = 1$ m and the geometry in Fig. 2. The frequency is 10 GHz. The results are presented in $\sigma_{hh}, \sigma_{hv}, \sigma_{vh}$ and σ_{vv} polarization in dBsm (decibels relative to one square meter).

5.1 Flat plate

The polarization dependent radar backscatter cross section in Fig. 7a is the result of the hh polarization. A maximum value of radar cross section is -19.58 dBsm and is in the middle of the calculation model (when SAR is closest to the scatter) and drops off sharply when the antenna away from the center of the geometry. The result of σ_{vv} in Fig. 7d has the similar curve as the result of σ_{hh} with the maximum value -22.59 dBsm. The maximum values of σ_{hv} and σ_{vh} in Fig. 7b and c are -75.97 dBsm and -337.4 dBsm, respectively. Although the values of σ_{vh} are very small. There are also regarded as interesting aspects of this cross-polar polarization.

5.2 Dihedral

Figure 8 shows the overall simulation results of a dihedral corner reflector of singly, doubly and triply reflected fields. The curving structures of co-polar polarization σ_{hh} and σ_{vv} in Fig. 8a and d have reached the maximum values in the middle of the simulation geometry with -13.56 dBsm and -16.57 dBsm, respectively. The maximum value of σ_{hv} in Fig. 8b in this configuration is -36.73 dBsm and the maximum value of σ_{vh} in Fig. 8d is -42.33 dBsm.

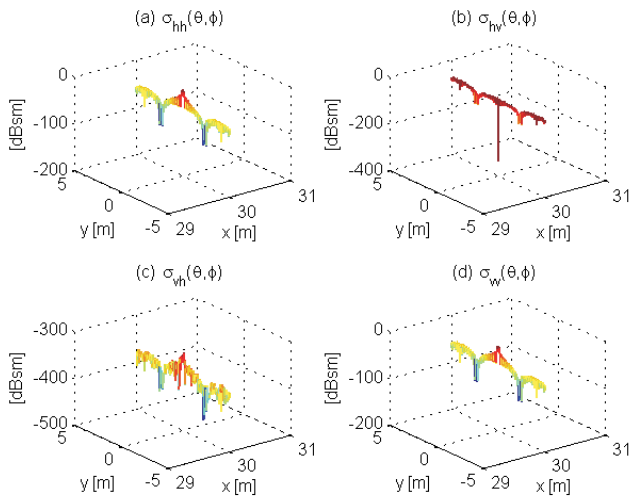


Fig. 7. Radar cross section of flat plate in (a) σ_{hh} ; (b) σ_{hv} ; (c) σ_{vh} and (d) σ_{vv} polarization.

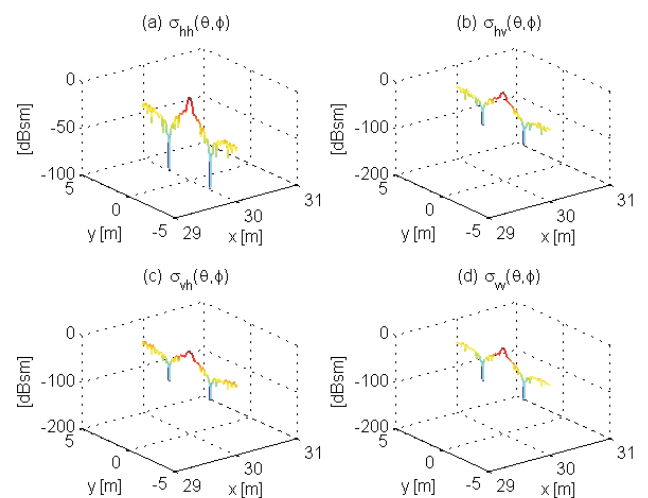


Fig. 9. Radar cross section of trihedral corner reflector in (a) σ_{hh} ; (b) σ_{hv} ; (c) σ_{vh} and (d) σ_{vv} polarization.

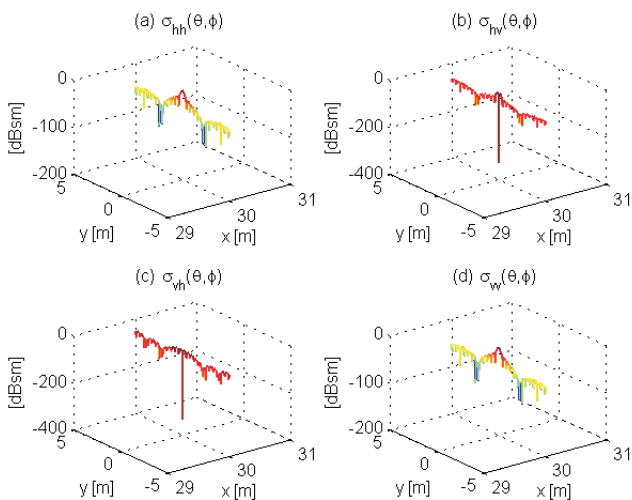


Fig. 8. Radar cross section of dihedral corner reflector in (a) σ_{hh} ; (b) σ_{hv} ; (c) σ_{vh} and (d) σ_{vv} polarization.

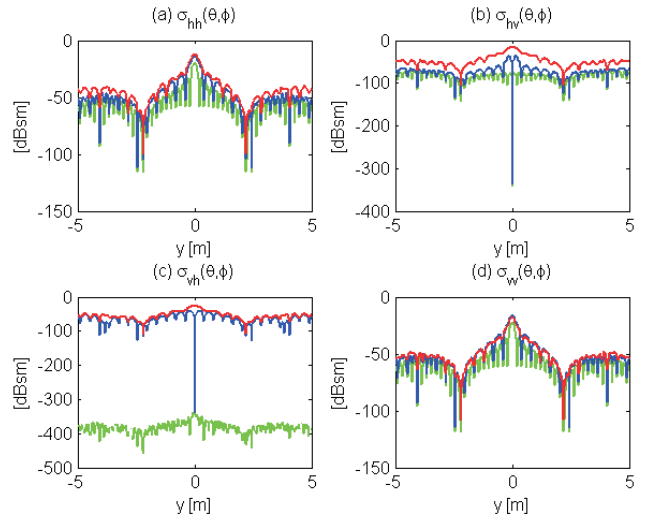


Fig. 10. Radar cross section of flat plate (green), dihedral (blue) and trihedral (red) corner reflector in (a) σ_{hh} ; (b) σ_{hv} ; (c) σ_{vh} and (d) σ_{vv} polarization.

5.3 Trihedral

Trihedral corner reflectors are commonly used as calibration targets or as a reference point in radar remote sensing. In this paper, the square trihedral corner reflector is used to evaluate the polarimetric radar cross section and the simulation results are presented in Fig. 9. Despite the similar curves of simulation results, there are different maximum values between each polarisation as follows: -12.54 dBsm, -15.89 dBsm, -26.63 dBsm and -17.79 dBsm for σ_{hh} , σ_{hv} , σ_{vh} and σ_{vv} in Fig. 9a, b, c and d, respectively.

Figure 10 presents the comparison of simulation results of flat plate (green line), dihedral (blue line) and trihedral (red line) corner reflector of each polarization. Because the radar backscatter cross section is in addition to the frequency

strongly dependent on the aspect angle, the simulation results were calculated by using the SAR geometry which poses different directions for the incident and scattered waves. An important point to note is that the difference between the scattering maxima of each target conforms with standard theory, thus confirming the validity of the calculations.

6 Conclusions

In the first part of this paper, we have provided a short review of electric field in wave propagation, radar cross section and simulation of scattered fields using physical optic. The new approach was developed to evaluate polarimetric radar cross

section under SAR geometry. In this paper, three scatter objects, i.e., flat plate, dihedral and trihedral corner reflector, are used to demonstrate the capability of the new approximation. The findings indicate that the SAR geometry has a large effect on backscatter cross section, because of continuously angle change during the observation time. Further work will also include the development of improved simulation method and target modelling for a better accuracy radar cross section, in particular the simulation efficiency.

References

- Lee, J. S. and Pottier, E.: Polarimetric Radar Imaging from Basics to Applications, CRC Press, Boca Raton, 2009.
Balanis, C. A.: Advanced engineering electromagnetics, John Wiley & Sons, Canada, 1989.